A level set approach for Left Ventricle detection in CT images using shape segmentation and optical flow

Jorge Brieva[a], Ernesto Moya-Albor[a] and Boris Escalante-Ramírez[b];

[a] Fac. de Ingeniería, Universidad Panamericana, Augusto Rodin 498, 03920 México, D.F.
[b] Fac. de Ingeniería, Dep. de Procesamiento de Señales, Edif. de Posgrado e Investigación, Universidad Nacional Autónoma de México, Cd. Universitaria, 04510 México, D.F.

ABSTRACT

The left ventricle (LV) segmentation plays an important role in a subsequent process for the functional analysis of the LV. Typical segmentation of the endocardium wall in the ventricle excludes papillary muscles which leads to an incorrect measure of the ejected volume in the LV. In this paper we present a new variational strategy using a 2D level set framework that includes a local term for enhancing the low contrast structures and a 2D shape model. The shape model in the level set method is propagated to all image sequences corresponding to the cardiac cycles through the optical flow approach using the Hermite transform. To evaluate our strategy we use the Dice index and the Hausdorff distance to compare the segmentation results with the manual segmentation carried out by the physician.

Keywords: level sets, left ventricle, shape model, optical flow, hermite transform

1. INTRODUCTION

Due to the fact that segmentation in medical images is still a challenging problem, numerous algorithms have been proposed. Such algorithms aim to solve this important stage for the subsequent higher-level analysis. For instance, characterization of an organ in an image. Segmentation methods can be divided in a general manner into two categories: those requiring strong prior knowledge and those requiring weak or no prior knowledge. The first one are more robust but require a learning phase which depends on the quality of the samples, making them less general. On the other hand, the second ones are in most cases less robust but they can be adapted to a more general scenarios.

Deformable models and their implementation by level sets proposed by Osher and Paragios[1] have been widely used in medical image segmentation.[2] Deformable models rely on the idea that a curve from a given image, subject to some constraints, can evolve in order to detect objects. According to the image features used to handle the curve evolution, they can be categorized as edge based,[3] region based[4,5] and model shape based.[?,6,7] An extension of the method for vector-value images was proposed by Chan et al.[8] and applied to color images. Additionally, Paraggios et al.[9] applied it to supervised texture segmentation problems. The vector value extension allows to introduce different kinds of features at the same time without requiring any prior knowledge. For example, Brox et al.[10] introduced simultaneously texture features, gray level and optic flow for the segmentation process. Vector value extensions aplied to left ventricular segmentation are presented in.[?]

Heart left ventricle has a circular aspect from the short axis view. Also right and left ventricular motions can be visualized from the short axis view and it is the basis for volumetric measurements used in global ventricular function evaluation. Typical segmentation of the endocardium wall in the left ventricle excludes papillary muscles which leads to an incorrect measure of the ejected volume. If the final segmentation includes most part of such muscles, we could get a more precise measure of the total blood volume.

Send correspondence to J.B.
J.B.: E-mail: jbrieva@up.edu.mx,Telephone: +52 55 5482 1600 Ext. 5267
E.M.A.: E-mail: emoya@up.edu.mx
B.E.R.: E-mail: boris@servidor.unam.mx

10th International Symposium on Medical Information Processing and Analysis,
edited by Eduardo Romero, Natasha Lepore, Proc. of SPIE Vol. 9287, 92870K

We used the level set approach based on the Chan Vese model[4] , with prior information, for LV segmentation in CT images, in order to propose a new strategy that combines a global region term and a local edge term to refine the segmentation of the endocardium wall. Aditionally, we update the shape model by means of the optic flow computed by means of the Hermite transform.

2. METHODS

2.1 Overview of approach

Let a sequence of M CT 2D images of left ventricle given by $\{L_1, ..., L_i, ..., L_M\}$ (corresponding to the cardiac cycles) the proposed level set segmentation method is divided into three steps: first, a segmentation of the image L_1 is carried out using a manual shape model defined by the user (Equation 5 is updated), second, the shape model is propagated from the L_i frame to the L_{i+1} frame by means of an optical flow strategy(Section2.3). Third, the level set Equation 5 is used. The shape model helps to handle the curve evolution in the level set equation and thus prevents the detection of other structures. This procedure is carried out on the M 2D images.

2.2 Segmentation using Level Sets

A level set formulation method based on Chan and Vese model is used to segment the Left Ventricle in each 2D frame of the image sequence. Let $\phi : \Omega \longrightarrow \mathcal{R}$ be a level set formulation on the domain Ω. An energy functional is defined as:

$$\varepsilon(\phi) = \varepsilon_G(\phi) + \varepsilon_L(\phi) + \varepsilon_S(\phi) \tag{1}$$

$\varepsilon_G(\phi)$ is a global term adopted from the Chan Vese model:

$$\varepsilon_G(\phi) = \mu \int_\Omega \delta(\phi) |\bigtriangledown \phi| \, dx + \lambda_1 \int_\Omega |L_i - c_1|^2 H(\phi) dx + \lambda_2 \int_\Omega |L_i - c_2|^2 H(-\phi) dx \tag{2}$$

where μ,λ_1,λ_2 are weighting factors, c_1 and c_2 are the averages intensities of the areas inside and outside of the active contour respectively. The Dirac delta function δ and the Heaviside function H are aproximated by expressions used by Chan et al.[8] We add a local term in a narrowband level set function defined by ϕ_N inside and outside the active contour. This term is defined by:

$$\varepsilon_L(\phi_N) = \lambda_3 \int_{\phi_N} |L_{E_i} - m_1|^2 H(\phi_N) dx + \lambda_4 \int_{\phi_N} |L_{E_i} - m_2|^2 H(-\phi_N) dx \tag{3}$$

L_{E_i} is a enhanced version of the image L_i, m_1 and m_2 are the average intensities of the areas defined on the narrow band ϕ_N. The enhanced version is computed for each pixel on a local window. In addition, we add a shape model ϕ_S (ϕ_S is the shape model recovered from the L_{i-1} frame by means of the optical flow strategy) constraint given by:

$$\varepsilon_S(\phi) = \gamma \int_\Omega (\phi - \phi_S)^2 \delta(\phi) \tag{4}$$

Then, keeping c_1, c_2, m_1 and m_2, derivating $\varepsilon(\phi)$ with respect to the fonction ϕ such that $G(\phi) = \frac{\partial \varepsilon(\phi)}{\partial \phi}$, a solution of $G(\phi)$ can be obtained asymptotically in t by resolving $\frac{\partial \phi}{\partial t} = G(\phi)$:

$$\begin{aligned}\frac{\partial \phi}{\partial t} =& \delta(\phi) \left(\frac{\bigtriangledown \phi}{|\bigtriangledown \phi|} - \lambda_1 (L_i - c_1)^2 + \lambda_2 (L_i - c_2)^2 \right)_{(x,y)\in\Omega} + \left(\beta \left(-\lambda_3 (L_{E_i} - m_1)^2 + \lambda_4 (L_{E_i} - m_2)^2 \right) \right)_{(x,y)\in\phi_N} + \\ &+ 2\gamma (\phi - \phi_S) \delta(\phi)\end{aligned} \tag{5}$$

2.3 Optical Flow

The optical flow (OF) is a way to determinate the apparent velocities that can be associated with a variation of brightness patterns in a sequence of images. Usually it can be represented in CT images by a vector field induced by the motion due to the change in position of different cardiac structures, which encodes the displacement of each pixel in the image.

Different methods have been proposed to recovery the motion in a sequence of images where the differential methods are the techniques with better performance. Differential methods are based on the work of Horn and Schunck[11] and Lucas and Kanade[12] both of 1981, which incorporated certain constraints in order to handle the Ill–posed problem of *Optical Flow Constraint* equation, where the data only calculated the normal component of motion:

$$uL_x + vL_y + L_t = 0 \tag{6}$$

where $L(x, y, t)$ be a image sequence, (x, y) represents the location within a rectangular image domain t denotes time and $L_* := \frac{\partial L}{\partial *}$.

In Moya-Albor et al.[13] we proposed a functional that included local image constraints using the Hermite transform. Our proposal is based on the polynomial decomposition of each of the images using the steered Hermite transform as a representation of the local characteristics of images from an perceptual approach within a multiresolution scheme.

Our contribution includes local restrictions using the steered Hermite transform as a representation of the local image characteristics from an perceptual approach. In[14] the effect of different local restrictions on the data term (intensity, gradient, Hessian, Laplacian) is described, but in our approach the steered Hermite coefficients allow including polynomial decomposition of the image and take these parameters as constraints that include intensity and higher order derivatives, which are useful to analyze the image in a similar way as is done by the HVS. The use of Gaussian derivatives allows incorporating image structure information from neighboring pixels that is robust to noise.[12,15] This feature is incorporated in a global differential functional that allows obtaining dense flow fields.[11,16]

The Hermite transform[17,18] is a special case of polynomial transform and it can be considered as an image description model. This is obtained by performing a convolution of the image $L(x, y)$ with the filter functions $D_{m,n-m}(x, y)$:

$$\begin{aligned} &L_{m,n-m}(x_0, y_0) = \int_{-\infty}^{\infty}\int_{-\infty}^{\infty} L(x, y)D_{m,n-m}(x_0 - x, y_0 - y)dxdy \\ &n = 0, 1, \ldots, \infty \\ &m = 0, 1, \cdots, n \end{aligned} \tag{7}$$

where $D_{m,n-m}(x, y)$ are the Hermite filter functions, $L_{m,n-m}(x, y)$ are the Hermite coefficients, and m and $(n - m)$ denote the analysis order in x and y direction respectively.

The local information for each analysis window in the convolution is expanded in terms of a family of orthogonal polynomials, with respect to the window function, $G_{m,n-m}(x, y)$ of m degree in x and $(n - m)$ in y.

Thus, from a perceptual standpoint and according to the scale-space theory, our option would be a Gaussian window, where adjacent Gaussian windows separated by twice the standard deviation σ are a good model of overlapping receptive fields found in physiological experiments.[19,20]

Using the Gaussian window:

$$v^2(x, y) = \left(\frac{1}{\sigma\sqrt{\pi}} \exp\left(-\frac{(x^2 + y^2)}{2\sigma^2}\right)\right)^2 \tag{8}$$

the associate Hermite polynomials are:

$$G_{m,n-m}(x, y) = \frac{1}{\sqrt{2^n m!(n - m)!}} H_m\left(\frac{x}{\sigma}\right) H_{n-m}\left(\frac{y}{\sigma}\right) \tag{9}$$

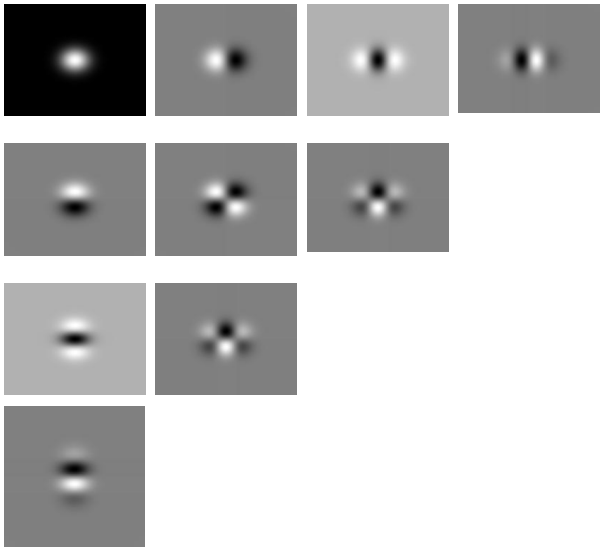

Figure 1. The Hermite filters $D_{m,n-m}(x,y)$ for $N=3$ ($n=0,1,\ldots,N$ and $m=0,1,\cdots,n$). $\begin{bmatrix} D_{0,0} & D_{1,0} & D_{2,0} & D_{3,0} \\ D_{0,1} & D_{1,1} & D_{2,1} & \\ D_{0,2} & D_{1,2} & & \\ D_{0,3} & & & \end{bmatrix}$

where $H_n\left(\frac{x}{\sigma}\right)$ represents the generalized Hermite polynomials with respect to the Gaussian function (with variance σ^2) given by Rodrigues' formula:

$$H_n\left(\frac{x}{\sigma}\right) = (-1)^n \exp\left(-\frac{x^2}{\sigma^2}\right) \frac{d^n}{dx^n} \exp\left(-\frac{x^2}{\sigma^2}\right) \tag{10}$$

The Hermite filters $D_{m,n-m}(x,y)$ (Fig. 1) are determined by:

$$D_{m,n-m}(x,y) = G_{m,n-m}(-x,-y)v^2(-x,-y) \tag{11}$$

A steered version of Hermite transform is obtained by a projection of the Hermite coefficients in terms of the orientation selectivity θ, the Hermite filters at each position in the image are adapted to local content:[21]

$$l_{m,n-m,\theta}(x_0,y_0) = \sum_{k=0}^{n} L_{k,n-k}(x_0,y_0) g_{k,n-k}(\theta) \tag{12}$$

where $g_{m,n-m}(\theta) = \sqrt{\binom{n}{m}}\left(\cos^m(\theta)\right)\left(\sin^{n-m}(\theta)\right)$ are the cartesian angular functions of order n that expresses the directional selectivity of the filter and $l_{m,n-m,\theta}(x_0,y_0)$ are the steered Hermite coefficients.

Our global energy functional penalizes deviations from the constancy in the polynomial decomposition of degree N ($n=1,2,\cdots,N$) of images including the coefficient of order 0 ($L_0 = L_{0,0}$) as a *Constant Intensity Constraint* and *Steered Hermite Coefficient Constraint* ($l_{n,\theta}$) within an non–linear multiresolution approach:

$$\begin{aligned} E(u,v) = &\int_\Omega \Psi\left(\left|L_0(x+u,y+v) - L_0(x,y)\right|^2 + \gamma\Big(\sum_{n=1}^{N}\left|l_{n,\theta}(x+u,y+v) - l_{n,\theta}(x,y)\right|^2\Big)\right) dxdy \\ &+\alpha \int_\Omega \Psi\Big(|\nabla u|^2 + |\nabla v|^2\Big) dxdy \end{aligned} \tag{13}$$

where $\Psi(s^2) = \sqrt{(s^2+\epsilon^2)}$ is the modified $\ell 1^*$–norm which is robust in the presence of flow discontinuities.[22] u and v are the displacement of a pixel at position (x,y) within the sequence of images at a time t to a time $(t+1)$ in the directions x and y respectively.

Table 1. Dice index and Hausdorff distance for Gray Level segmentation, Optical Flow segmentation and Shape Model segmentation

Time	Segmentation					
	Gray level		Optical flow		Shape Model	
(%)	Dice	Hausdorff	Dice	Hausdorff	Dice	Hausdorff
10	0.8980	40.6296	0.9619	12.6661	0.9504	13.4141
20	0.8794	43.2273	0.9358	11.1122	0.9474	14.5000
30	0.8018	46.9682	0.9546	9.1285	0.9577	10.5000
40	0.7585	45.1296	0.9070	13.8559	0.9474	8.1394
50	0.7733	45.6098	0.8986	20.178	0.9440	13.8293
60	0.7586	46.1635	0.8739	19.3499	0.9173	13.0863
70	0.8850	37.8054	0.9564	7.4523	0.9626	6.5000
80	0.8633	36.5508	0.9565	7.5428	0.9544	8.3265

3. RESULTS

For the experiments, we used cardiac computed tomography studies from two patients. Such studies were performed on a CT Siemens dual source scanner with 128 channels. Each study contains 10 volumes that correspond to the time percentage of the cardiac cycle.

We present the obtained segmentation results for one patient in all the percentages of cardiac cycles in Fig. 2 and the accuarcy results of the methods in Table 1. In Fig. 2 column 1 shows the reference segmentation performed by the physician, column 2 shows the segmentation using the Chan Vese model, column 3 shows the updating shape using optical flow and column 4 shows the shape model level set approach.

To evaluate the segmentation performance we use the Dice index and the Hausdorff distance. This metrics are widely used in the litterature to measure accuracy of the segmentation.[7] The Dice metric d_D is a measure of contour overlap between the reference and the segmentation results. The Dice value ranges between 0 and 1. Values close to 1 indicate more similar contours. Moreover, the Hausdorff distance, d_H, measures how close a point from a reference set is from another point of the segmentation set in a metric space. Hausdorff minimal values indicate more alike boundaries in a range from 0 to 100.

In these results (Table 1) we notice notice that, first the deformation produced by the optical flow to the shape model evolve acording to the reference segmentation performed by the physician, second, that by introducing the shape model in the level set equation the segmentation results are inproved significantly in comparison to the classical method without shape model. We observe that in the cardiac time percentage cycles corresponding to major myocardial contraction (40 % to 70%), both, the Dice index and the Hausdorff distance correspond to better results in the shape model segmentation method comparing to the optical flow deformation and in the other cardiac time percentage cycles the metrics values are comparables.

4. CONCLUSIONS

In this work, we present a new strategy for extracting the LV from cardiac CT images with leak prior knowledge. We use a local term in the Chan Vese model for enhancing the low contrast structures as the edges of the papillary muscles and a shape model that is propagated in the image sequence by means of a robust optical flow strategy using the Hermite transform. In this work, we used the temporal information to handle the shape model to introduce in the Level Set equation. With this strategy, we will compute easily the deformation of the contour. We have obtained preliminary results on a cardiac CT sequence.This algorithm will be tested in more patients for an accurate validation.

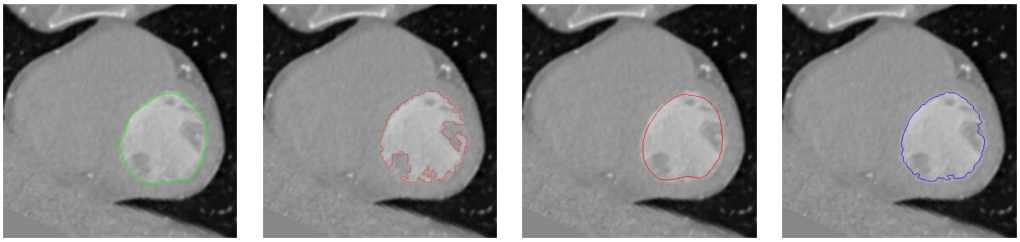

(a) Reference 20% (b) Gray-LS 20% (c) OF 20% (d) Shape-Model 20%

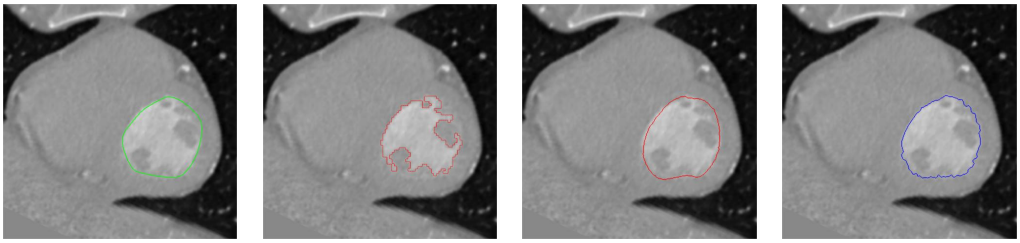

(e) Reference 30% (f) Gray-LS 30% (g) OF 30% (h) Shape-Model 30%

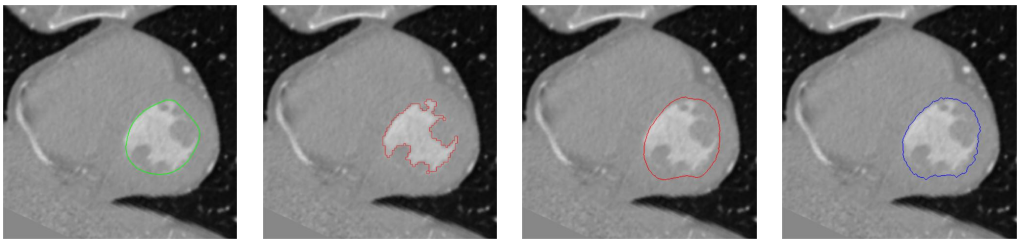

(i) Reference 40% (j) Gray-LS 40% (k) OF 40% (l) Shape-Model 40%

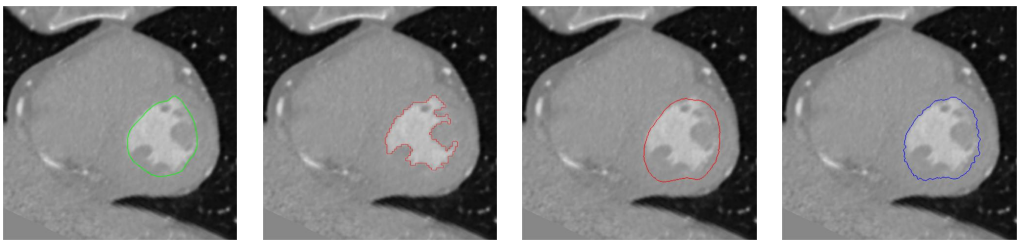

(m) Reference 50% (n) Gray-LS 50% (o) OF 50% (p) Shape-Model 50%

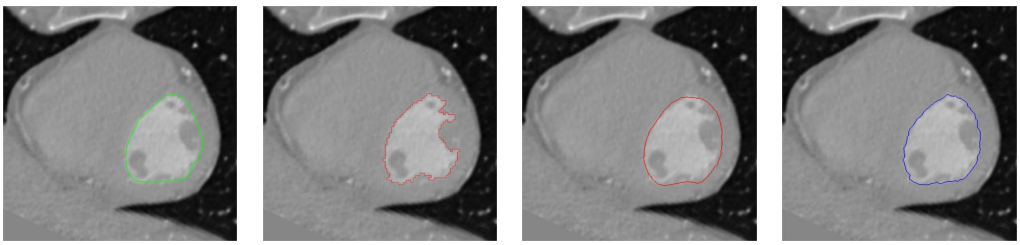

(q) Reference 70% (r) Gray-LS 70% (s) OF 70% (t) Shape-Model 70%

Figure 2. column 1 we show physician reference, columne 2 Chan Vese model segmentation, column 3 updated model by optical flow, column 4 whole strategy

ACKNOWLEDGEMENTS

Jorge Brieva and Ernesto Moya-Albor would like to thank the Facultad de Ingeniera of Universidad Panamericana for all support in this work.

Boris Escalante-Ramírez gives a special thank to UNAM for PAPIIT grant IG100814.

The authors wish to thank to Enrique Vallejo M.D. of Hospital Angeles del Pedregal (Mexico) for the CT images that were presented in this paper and Jimena Olveres Montiel PhD student of UNAM (Mexico) for performing the short axis projections.

REFERENCES

[1] Osher, S. and Paragios, N., [*Geometric Level Set Methods in Imaging,Vision,and Graphics*], Springer-Verlag New York, Inc., Secaucus, NJ, USA (2003).

[2] Suri, J., Liu, K., Singh, S., Laxminarayan, S., Zeng, X., and Reden, L., "Shape recovery algorithms using level sets in 2-d/3-d medical imagery: a state-of-the-art review," *Information Technology in Biomedicine, IEEE Transactions on* **6**(1), 8–28 (2002).

[3] Caselles, V., Kimmel, R., and Sapiro, G., "Geodesic active contours," *Int. J. Comput. Vision* **22**, 61–79 (Feb. 1997).

[4] Chan, T. and Vese, L., "Active contours without edges," *Image Processing, IEEE Transactions on* **10**, 266–277 (Feb 2001).

[5] Gao, S. and Bui, T., "Image segmentation and selective smoothing by using mumford-shah model," *IEEE Transactions on Image Processing* **14**(10), 1537–1549 (2005).

[6] Huang, C.-L., "Shape-based level set method for image segmentation," in [*Ninth International Conference on Hybrid Intelligent Systems*], **1**, 243–246 (2009).

[7] Kohlberger, T., Uzunba, M., Alvino, C., Kadir, T., Slosman, D., and Funka-Lea, G., "Organ segmentation with level sets using local shape and appearance priors," in [*Medical Image Computing and Computer-Assisted Intervention (MICCAI)*], Yang, G.-Z., Hawkes, D., Rueckert, D., Noble, A., and Taylor, C., eds., *Lecture Notes in Computer Science* **5762**, 34–42, Springer Berlin Heidelberg (2009).

[8] Chan, T. F., Sandberg, B. Y., and Vese, L. A., "Active contours without edges for vector-valued images," *Journal of Visual Communication and Image Representation* **11**, 130–141 (2000).

[9] Paragios, N. and Deriche, R., "Geodesic active regions: A new framework to deal with frame partition problems in computer vision," *Journal of Visual Communication and Image Representation* **13**(1-2), 249–268 (2002).

[10] Brox, T., Rousson, M., Deriche, R., and Weickert, J., "Colour, texture, and motion in level set based segmentation and tracking," *Image and Vision Computing* **28**(3), 376 – 390 (2010).

[11] Horn, B. K. P. and Schunck, B. G., "Determining Optical Flow," *Artificial Intelligence* **17**(1-3), 185–203 (1981).

[12] Lucas, B. D. and Kanade, T., "An Iterative Image Registration Technique with an Application to Stereo Vision," in [*Proceedings of the Seventh International Joint Conference on Artificial Intelligence (IJCAI '81)*], 674–679 (April 1981).

[13] Moya-Albor, E., Escalante-Ramírez, B., and Vallejo, E., "Optical flow estimation in cardiac CT images using the steered Hermite transform," *Signal Processing: Image Communication* **28**(3), 267–291 (2013).

[14] Papenberg, N., Bruhn, A., Brox, T., Didas, S., and Weickert, J., "Highly accurate optic flow computation with theoretically justified warping," *International Journal of Computer Vision* **67**, 141–158 (April 2006).

[15] Bigün, J., Granlund, G., and Wilklund, J., "Multidimensional orientation estimation with applications to texture analysis and optical flow," *IEEE Trans. on Pattern Analysis and Machine Inteligence* **13**(8), 775–790 (1991).

[16] Nagel, H.-H., "Constraints for the estimation of displacement vector fields from image sequences," in [*International Joint Conference on Artificial Intelligence*], 945–951 (1983).

[17] Martens, J.-B., "The hermite transform–theory," *IEEE Transactions on Acoustics, Speech and Signal Processing* **38**(9), 1595–1606 (1990).

[18] Martens, J.-B., "The hermite transform–applications," *IEEE Transactions on Acoustics, Speech and Signal Processing* **38**(9), 1607–1618 (1990).
[19] Sakitt, B. and Barlow, H., "A model for the economical encoding of the visual image in cerebral cortex," *Biological Cybernetics* **43**(2), 97–108 (1982).
[20] Levine, M. D., [*Vision in Man and Machine*], McGraw-Hill, New York (1985).
[21] van Dijk, A. M. and Martens, J.-B., "Image representation and compression with steered Hermite transforms," *Signal Processing* **56**(1), 1–16 (1997).
[22] Bruhn, A., Weickert, J., and Schnörr, C., "Lucas/Kanade Meets Horn/Schunck: Combining Local and Global Optic Flow Methods," *International Journal of Computer Vision* **61**(3), 211–231 (2005).